

Dielectrophoretic-activated cell sorter based on curved microelectrodes

Khashayar Khoshmanesh · Chen Zhang ·
Francisco J. Tovar-Lopez · Saeid Nahavandi ·
Sara Baratchi · Arnan Mitchell · Kourosh Kalantar-Zadeh

Received: 22 October 2009 / Accepted: 10 December 2009 / Published online: 29 December 2009
© Springer-Verlag 2009

Abstract This article presents the numerical and experimental analysis of a dielectrophoretic-activated cell sorter (DACS), which is equipped with curved microelectrodes. Curved microelectrodes offer unique advantages, since they create strong dielectrophoretic (DEP) forces over the tips and maintain it over a large portion of their structure, as predicted by simulations. The performance of the system is assessed using yeast (*Saccharomyces cerevisiae*) cells as model organisms. The separation of the live and dead cells is demonstrated at different medium conductivities of 0.001 and 0.14 S/m, and the sorting performance was assessed using a second array of microelectrodes patterned downstream the microchannel. Further, microscopic cell counting analysis reveals that a single pass through the system yields a separating efficiency of $\sim 80\%$ at low medium conductivities and $\sim 85\%$ at high medium conductivities.

Keywords Dielectrophoresis · Microfluidics · Yeast · Sorting

1 Introduction

The emergence of micro/nano technologies have enabled us to develop systems, which can efficiently manipulate, separate, monitor and treat biological cells (Baratchi et al. 2009; Castillo et al. 2009; El-Ali et al. 2006; Khoshmanesh et al. 2008). Such systems employ mechanical, acoustic, electrical (electrophoresis and dielectrophoresis), magnetic, thermal, optical and chemical phenomena within microfluidic units, as reviewed comprehensively in (Andersson and van den Berg 2003; Castillo et al. 2009; Roda et al. 2009; Zhang et al. 2010). Amongst these phenomena, dielectrophoresis can be efficiently employed in exploiting the dielectric properties of particles within the suspension. These properties are closely relevant to particles' structures and compositions which are crucial factors for their manipulations (Gascoyne and Vykoukal 2004; Zhang et al. 2009).

Dielectrophoretic (DEP) force is generated when a neutral particle is suspended in a non-uniform electric field. The electric field induces electrical charges within the particle and form dipoles. In a non-uniform electric field, the ends of the dipole experience unequal Columbic forces and the resulting net force imposed on the particle is non-zero. If the particle is more polarizable than the suspending medium, then the particle is attracted towards the regions of higher electric field, and the motion is called positive dielectrophoresis. Conversely, if the particle is less polarizable than the suspending medium, then it is repelled from the regions of higher electric field, and the motion is called negative dielectrophoresis. Such motions that are caused by the gradient of electric field magnitude are called classical DEP motions. In addition, dielectrophoresis may also be caused by the gradient of phase of the applied electric field that is called travelling wave dielectrophoresis (Gascoyne

K. Khoshmanesh (✉) · S. Nahavandi
Centre for Intelligent Systems Research, Deakin University,
Geelong, VIC 3217, Australia
e-mail: kkho@deakin.edu.au

C. Zhang · F. J. Tovar-Lopez · A. Mitchell · K. Kalantar-Zadeh
School of Electrical and Computer Engineering, RMIT
University, Melbourne, VIC 3001, Australia

S. Baratchi
Institute of Biotechnology (BioDeakin), Deakin University,
Geelong, VIC 3217, Australia

and Vykoukal 2004). Dielectrophoresis has been widely applied in different biological applications. It has been utilized to detect, separate, manipulate and characterize biological particles including cells (Gray et al. 2004; Hashimoto et al. 2009; Pethig and Talarly 2007; Urdaneta and Smela 2007), bacteria (Hoettges et al. 2007; Hu et al. 2005; Moon et al. 2009; Sanchis et al. 2007); virus (Morgan et al. 1999, 2007), parasites (Dalton et al. 2004; Gascoyne et al. 2004), DNA molecules (Hoeb et al. 2007; Kuzyk et al. 2008) and cell organelles (Radu et al. 2005; Uppalapati et al. 2008).

Properties of yeast cells have made them an attractive benchmark in the dielectrophoresis research, and they have been used to implement many novel concepts. In one of the first reports, the manipulation of yeast cells by means of DEP forces was described by Crane and Pohl (Crane and Pohl 1968). Since then, different DEP systems have been introduced with the capability of patterning and manipulation of yeast cells (Arnold and Franich 2006; Kadaksham et al. 2005; Morales et al. 2008), the separation of the live from dead yeast cells (Arnold 2001; Fatoyinbo et al. 2005; Li et al. 2007; Markx et al. 1994) and yeast cells from polystyrene microparticles (Bhatt et al. 2005; Hunt et al. 2004; Lee et al. 2007). Fu et al. (2004) applied the travelling wave DEP force rather than the classical DEP force to manipulate the yeast cells. Abidin and Markx (2005) developed an electrodeless DEP system to separate the yeast cells, in which glass beads were placed within the microchannel to distort the electric field and create regions of high electric fields. Urdaneta and Smela (2007) employed a multiple frequency DEP system, in which each microelectrode was excited at a different frequency. Using this concept, the live and dead yeast cells could be trapped at different microelectrodes concurrently. Kua et al. (2007) developed a DEP system to simultaneously transport and fractionate the live and dead yeast cells. Their system was equipped with arrays of microelectrodes that were excited independently. The transportation of cells was controlled by the interelectrode inactivation time while the fractionation of cells was controlled by the applied frequency. Cetin et al. (2009) and Kang et al. (2009) developed DEP systems equipped with 3D microelectrodes to separate yeast cells from white blood cells and polystyrene microparticles, respectively. In those studies, metallic microelectrodes were embedded along the sidewalls of microchannels to create a DEP field. In other studies, complementary elements were integrated to DEP platforms to make them more versatile. For example, Wang et al. (2006) integrated polymeric optical elements (waveguides, lens and fibre coupler) to a DEP platform to measure the light scattered by the yeast cells. Using this system, the live and dead yeast cells were separated, and the sorting efficiency was monitored online. Hunt et al. (2008) applied an

integrated circuit to control a large array of pixel microelectrodes embedded within a DEP platform. Using this system, thousands of yeast cells could be moved and trapped by means of a microfluidic chamber.

In this study, we present a DEP-activated cell sorter to manipulate and separate model live and dead yeast cells. While many researchers have applied arrays of parallel microelectrodes (Li et al. 2007), castellated microelectrodes (Kadaksham et al. 2005; Morales et al. 2008; Wang et al. 2006) or extruded posts (Hunt et al. 2004; Lee et al. 2007) to manipulate the yeast cells, the system proposed in this study takes advantage of curved microelectrodes. Numerical simulations reveal that the curved microelectrodes create a strong electric field over the tips and maintain it along a large portion of their structure imposing strong DEP forces on target cells. The DEP force is increased smoothly, avoiding undesirable motions at microelectrode tips. Separate experiments are conducted with the live and dead cells to explore the performance of the system and characterize the DEP response of cells at different frequencies and medium conductivities. The curved microelectrodes obtain a wide catchment area at the bottom surface of the microchannel, where the live cells can be trapped in dense populations. Therefore, compared to parallel (Li et al. 2007) and castellated (Kadaksham et al. 2005; Morales et al. 2008; Wang et al. 2006) microelectrodes, where the live cells are patterned along discrete locations of the microchannel, the curved configuration offers a more appropriate platform to analyse the trapped cells. Moreover, the separation of the live and dead cells are demonstrated at various medium conductivities of 0.001 and 0.14 S/m reflecting the different conditions experienced in biological experiments. The experiments demonstrate the capability of curved microelectrodes for the efficient separation of cells according to their dielectric properties. The efficiency of the system is assessed by a second array of microelectrodes patterned downstream the microchannel, offering a fully DEP-activated system for biological experiments. Further microscopic cell counting analysis reveals that a single pass through the system yields a separating efficiency of $\sim 80\%$ at low medium conductivities and $\sim 85\%$ at high medium conductivities.

2 Theoretical background

The yeast cells are not perfectly spherical and can be more accurately modelled as oblate spheroids. Furthermore, the polarization of the cell membrane under an external electric field exerts local forces (Krassowska and Neu 1994) which cause various deformational regimes of cell elongation (Kononenko and Shimkus 2000) and can transform the spherical cell into prolate ellipsoids if the membrane

surface is sufficiently flexible (Neek-Amal et al. 2009). However, for simplification, they are generally considered as spherical particles (Kadaksham et al. 2005; Urdaneta and Smela 2007). For a homogenous spherical particle, the time-averaged DEP force is given as below (Jones 2003):

$$\bar{F}_{\text{DEP}} = 2\pi r^3 \epsilon_{\text{medium}} \text{Re}[f_{\text{CM}}(\omega)] \nabla E_{\text{rms}}^2, \tag{1}$$

where r is the radius of the particle, ϵ is the permittivity, $\text{Re}[f_{\text{CM}}]$ is the real part of the Clausius–Mossotti (CM) factor and E_{rms} is the root-mean-square (rms) value of the electric field. The f_{CM} is calculated as follows:

$$f_{\text{CM-cell}} = \frac{\epsilon_{\text{cell}}^* - \epsilon_{\text{medium}}^*}{\epsilon_{\text{cell}}^* + 2\epsilon_{\text{medium}}^*}, \tag{2}$$

where ϵ^* is the complex permittivities of the cell and the medium defined as below:

$$\epsilon^* = \epsilon - \frac{i\sigma}{\omega}, \tag{3}$$

in which $i = \sqrt{-1}$, σ is the electric conductivity, and ω is the angular frequency of the electric field.

The $\text{Re}[f_{\text{CM}}]$ embodies five influential parameters of the dielectrophoresis as follows: (i) the dielectric properties of particles, (ii) the exterior shape of particles, (iii) the interior structure of particles, (iv) the dielectric properties of the suspending medium and (v) the applied frequency. The first three parameters exhibit the characteristics of the particle and enable the characterization/sorting of them. For example, the dielectric properties of viable and non-viable cells are different, and this distinction can be employed for sorting them. Alternatively, the last two parameters are mostly imposed by the user to maximize the performance of DEP systems. For example, the cells might demonstrate positive or negative DEP behaviours at certain frequency ranges. In this case, appropriate frequencies are set by the user to trap or repel the target cells. The cells are pushed towards or against the regions of high electric field, depending upon whether the $\text{Re}[f_{\text{CM}}]$ is positive or negative. The $\text{Re}[f_{\text{CM}}]$ given by Eq. 2 corresponds to a single-shell structure. For multi-shell structures, such as the yeast cells, the calculation procedure is more complicated, as will be described in Sect. 4.1.

3 Materials and methods

3.1 Principles of the demonstrated DEP system

Figure 1 presents the plan view of the proposed DEP system. The system consisted of a microchannel that was integrated onto a DEP platform. The microchannel was fabricated from PDMS (polydimethylsiloxane) with a width of 1,000 μm and thickness of 80 μm . The

microchannel took advantage of a $\text{Ø}6$ mm inlet reservoir to inject the suspensions. The DEP platform consisted of a glass substrate that supported ten pairs of microelectrodes arranged in two arrays on its surface. The first array served to manipulate/sort the cells, whereas the second array served to assess the sorting efficiency of the first array.

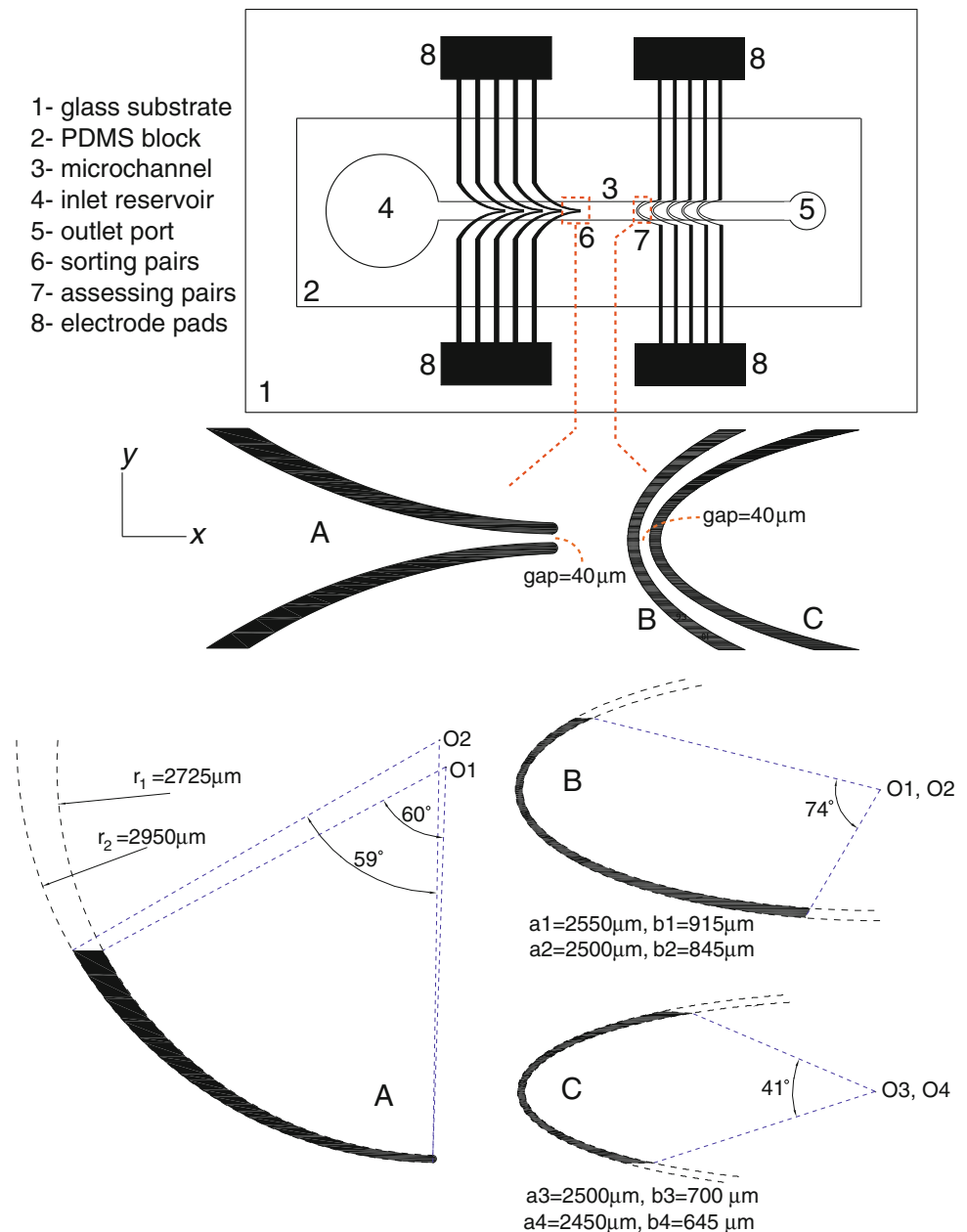
The first array took advantage of curved microelectrodes that were created by intersecting two circles of 2,725 and 2,950 μm radius with a distance of 185 μm between their centres, as shown in Fig. 1A. Under this combination, the width of the microelectrode was 200 μm at the base and decreased gradually along the surface until reaching 50 μm at the tip. The minimum gap between the opposite microelectrodes was set to 40 μm to create a strong electric field along the centreline while the distance between the consequent pairs was set to 1,000 μm to minimize their interference and the occupied space. The electric potential was applied through the pads of 6×2.25 mm, arranged on both sides of the microchannel. The microelectrodes laid on one side of the microchannel were grounded while the microelectrodes laid on the opposite side were excited with an AC signal. This arrangement obtained a strong electric field across the microchannel, which could effectively trap the viable cells between the pairs while repelling the non-viable cells towards the sidewalls.

Alternatively, the second array took advantage of boomerang-shaped microelectrodes that were created by intersecting two concentric ellipses, as shown in Fig. 1B and C. Each pair consisted of a larger boomerang (Fig. 1B) that encircled a smaller boomerang (Fig. 1C). Under this combination, the width of the microelectrode remained as 50 μm along the surface. The minimum gap between the opposite microelectrodes was set to 40 μm to create a strong electric field across the microchannel while the distance between the consequent pairs was set to 820 μm to minimize their interference and the occupied space. The microelectrodes were excited with an AC signal in an interdigitated manner, in which the larger microelectrodes were grounded while the smaller microelectrodes were excited with the AC potential. This arrangement obtained a strong electric field along the microchannel, which could effectively trap the viable cells between the pairs while retaining the non-viable cells behind the microelectrodes. Compared to parallel configuration (Gascoyne et al. 2009), the gap between the opposite microelectrodes was uneven across the microchannel (y -axis), beginning from 250 μm at the sidewalls and then decreasing to 40 μm at the centreline. This trend not only provided a larger trapping area along the sidewalls but also created a corridor for the retained non-viable cells to pass through the second array and not to block the microchannel, as later shown in experiments.

The performance of the curved microelectrodes strongly depends on its curvatures and the minimum gap between

Fig. 1 The layout of the DEP system, comprising of a PDMS microchannel integrated into the DEP platform, *A* curved configuration set for sorting array, and *B–C* boomerang-shaped configuration for assessing array

- 1- glass substrate
- 2- PDMS block
- 3- microchannel
- 4- inlet reservoir
- 5- outlet port
- 6- sorting pairs
- 7- assessing pairs
- 8- electrode pads



the pairs. In order to optimize our design, we examined the structure and performance of the curved microelectrodes by varying the radius of the inner edge (r_2 in Fig. 1A) in the range of 2,300–3,200 μm and the minimum gap (gap in Fig. 1A) in the range of 30–50 μm . According to our analysis, either decreasing of r_2 or gap, each led to the generation of sharp electric field gradients at the tips, weakening the electric field gradients over a large portion of the structure, decreasing the trapping area between the pairs and complicating the fabrication process. On the contrary, increasing either r_2 or gap resulted in the weakening of the electric field gradients at the tips, and increasing the length of the sorting array.

The curved microelectrodes have distinct advantages over parallel and oblique (Hu et al. 2005; Pommer et al. 2008) microelectrodes. In order to assess the benefits of curved microelectrodes, we compared the distribution of electric field in two DEP platforms equipped with oblique and curved microelectrodes. Except for their curvatures, all other geometrical specifications of the microelectrodes including the minimum gap between the opposing electrodes were the same, and they were subjected to a 30 V_{p-p} potential (equivalent to a magnitude of 10.6 V_{rms}). Simulation was conducted using Fluent 6.3 software package (Fluent, USA, Lebanon, NH) with details previously reported in (Khoshmanesh et al. 2009). Figure 2a and b

shows the contours of electric field (E_{rms}) at the bottom surface of the microchannel for oblique and curved configurations, respectively. The oblique microelectrodes created a strong electric field of 8.8×10^5 V/m over the tips, which sharply decreased along the structure and left the rest of the microelectrode with a moderate electric field. In contrast, the curved microelectrodes created an electric field of 7.6×10^5 V/m over the tips, which was 13.6% lower than that of oblique ones. However, the electric field decreased much smoother along the structure, which increased the effective portion of the microelectrodes for dielectrophoresis. A similar trend was observed in the other regions of the microchannel.

For more clarity, Fig. 2c depicts the variations of the electric field along three arbitrary lines within the microchannel. The dotted curves correspond to oblique configuration while the continuous curves correspond to curved configuration. Along all the lines, the high electric field region obtained by the oblique configuration was limited to a narrow area around the tips whereas the high electric field region obtained by the curved configuration was more consistent and maintained over a larger area. Furthermore, Fig. 2d compares the ∇E_{rms}^2 created by oblique and curved microelectrodes along an arbitrary line (Line 4). This variable is proportional to the induced DEP force, as given in Eq. 1 and generates positive or negative DEP force

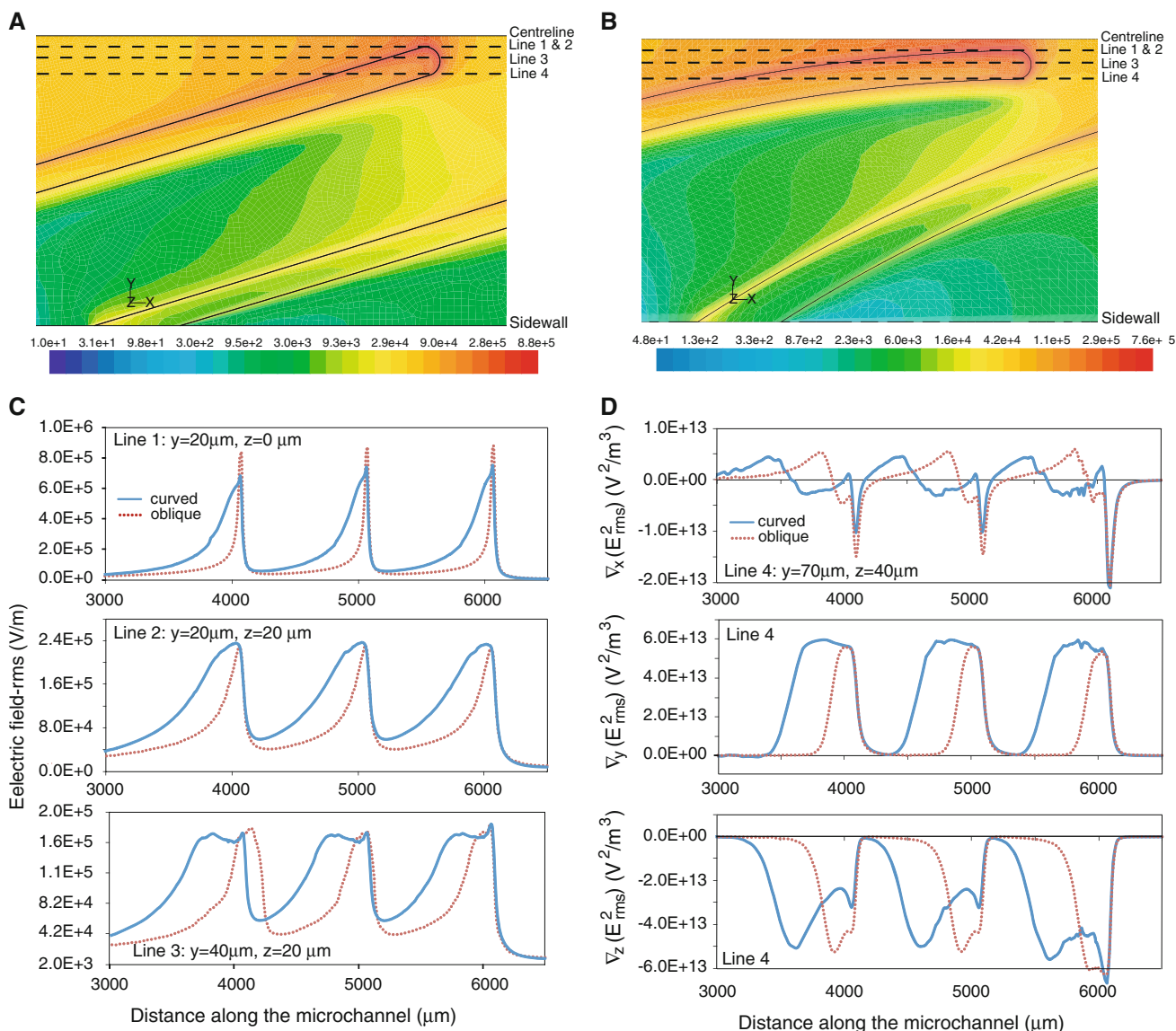


Fig. 2 The comparison of oblique and curved microelectrodes: **a, b** The electric field obtained at the bottom surface of the microchannel, where electrodes are patterned. **c** The variations of electric field (E_{rms}) along three arbitrary lines (lines 1–3). **d** The variations of ∇E_{rms}^2 along line 4

according to the sign of $Re[f_{CM}]$. The dotted curves correspond to oblique configuration while the continuous curves correspond to curved configuration. The DEP forces were repeated with a period of 1,000 μm , which corresponded to the distance between the consequential microelectrode pairs. The $\partial E_{rms}^2/\partial x$ fluctuated between positive and negative values, corresponding to acceleration/deceleration of cells at the tips depending on their positive/negative DEP responses. The mean value of this variable was -1.75×10^{10} and $-2.96 \times 10^{11} \text{ V}^2/\text{m}^3$ for oblique and curved configurations, respectively. This variable is not of great importance for us, since our experiments showed that the induced DEP- x force was much weaker than the hydrodynamic drag force and could not affect the travelling velocity of cells along the microchannel. Alternatively, the $\partial E_{rms}^2/\partial y$ was positive for both configurations, corresponding to pushing the cells towards/away from the tips depending on their positive/negative DEP responses. The mean value of this variable was 9.58×10^{12} and $2.44 \times 10^{13} \text{ V}^2/\text{m}^3$ for oblique and curved configurations, respectively, implying the superiority of curved configuration to push the cells along the y -axis. Instead, the $\partial E_{rms}^2/\partial z$ was positive for both configurations, corresponding to descending/ascending of the cells depending on their positive/negative DEP responses. The mean values of this variable was -1.28×10^{13} and $-2.03 \times 10^{13} \text{ V}^2/\text{m}^3$ for oblique and curved configurations, respectively, again implying the superiority of curved configuration to push the cells along the z -axis.

3.2 Fabrication process

In order to fabricate the DEP platform, thin films of chrome/gold were deposited on the surface of glass substrates using the electron beam evaporation process with a thickness of 500/1,500 \AA , respectively. The microelectrodes were patterned using photolithography techniques (Kalantar-Zadeh and Fry 2007). A thin film of AZ1512 (Clariant, USA) positive photoresist was spin coated on the substrate at a thickness of 1 μm . The sample was exposed to UV light using a mask aligner (Karl Suss MA6) and then developed. Finally, the additional chrome/gold film was etched using relevant etchants. Separately, the microchannel was made from PDMS using soft lithography techniques (Kalantar-zadeh and Fry 2007). A 3-inch diameter silicon wafer was used as the substrate and spin coated with KMPR (MicroChem Corporation) negative photoresist to a thickness of 80 μm . The sample was exposed to UV light using the MA6 mask aligner and developed with SU-8 developer. PDMS (SYLGARD 184, Dow Corning) was poured into the master to realize the microchannel. The resulting microchannel was assembled on the patterned glass substrate, and copper wires were

bounded to the microelectrode pads using silver-based epoxy glue. The DEP system was then sandwiched between two plexiglass cover slips to avoid leakage (Fig. 3).

3.3 Experimental setup

Instant-dried yeast powder (Tandaco, New South Wales, Australia) was used as the source of *Saccharomyces cerevisiae* yeast cells. First, the yeast cells were dissolved in 20 ml of DI water and centrifuged at 2,000g for 5 min. The supernatant was discharged and pellets were resuspended by pipetting. This procedure was repeated three times to eliminate the chemicals, such as emulsifier, vegetable gum or of ascorbic acid, which might adhere to the cell surface. In order to produce the live yeast solution, 150 mg of yeast powder was mixed with 40 ml of DI water and kept in a water bath for 30 min. Alternatively, to produce the dead yeast solution, 150 mg of yeast powder was mixed with 40 ml of a 50-50% DI water–methanol solution and kept in a water bath for 45 min. In order to stain the dead cells, 100 μl of Trypan blue (Sigma-Aldrich, USA) was added to 1,000 μl of the suspension and kept in a water bath for 10–15 min with occasional stirring. The plasma membrane and the surrounding walls of the dead cells were ruptured and let the stain penetrate the cell interior to make it blue.

In order to separate the live and dead cells, a mixture of 50–50% live–dead yeast cells with a total concentration of 5×10^7 cells/ml was prepared. Trypan blue exclusion assay indicated that >95% of the live cells were viable (not stained) while >85% of dead cells were non-viable (stained).

During the experiments, the relevant suspensions were injected to the inlet reservoir and were extracted through the outlet at desired flow rates, using a syringe pump (Harvard Apparatus, PHD 2000). The microchannel was observed using an inverted optical microscope (Nikon

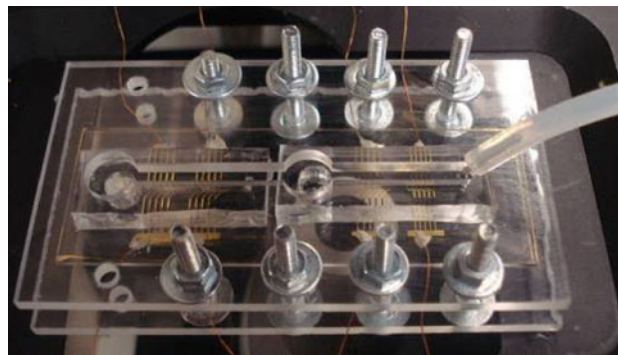


Fig. 3 The PDMS blocks were integrated into the DEP platform to make up the DEP system. The shown platform consisted of two separate DEP systems

Eclipse, TE 2000) to examine the performance of the system and the responses of the live and dead yeast cells. An oscillating signal was applied to the electrode pads using a function generator (Etabor Electronics, series 8200). The electrical conductivity of the medium was measured using a high precision conductivity meter (EC-Testr11+, Eutech Instruments).

4 Numerical analysis of DEP forces

4.1 Obtaining the $Re[f_{CM}]$ spectra of the live and dead yeast cells

Some DEP characterizations of yeast cells have been demonstrated by Huang et al. (1992) and Holzel (1997). Huang et al. (1992) approximated the structure of yeast cells by a spherical double-shell model comprising a cell interior, a plasma membrane and an outer wall and then measured the dielectric properties of the live and dead cells. In this study, the yeast cells were considered as double-shell structures as proposed in Huang et al. (1992), and their $Re[f_{CM}]$ spectra was calculated as suggested in Morgan and Green (2003). In doing so, the equivalent complex permittivities of the cell interior and plasma membrane were calculated using Eq. 4. The same procedure was applied to the outer wall to calculate the equivalent complex permittivity of the whole cell using Eq. 5:

$$\epsilon_{ci+pm}^* = \left(\left[\frac{r_{pm}}{r_{ci}} \right]^3 + 2 \left[\frac{\epsilon_{ci}^* - \epsilon_{pm}^*}{\epsilon_{ci}^* + 2\epsilon_{pm}^*} \right] \right) / \left(\left[\frac{r_{pm}}{r_{ci}} \right]^3 - \left[\frac{\epsilon_{ci}^* - \epsilon_{pm}^*}{\epsilon_{ci}^* + 2\epsilon_{pm}^*} \right] \right) \tag{4}$$

$$\epsilon_{cell}^* = \left(\left[\frac{r_{ow}}{r_{ci+pm}} \right]^3 + 2 \left[\frac{\epsilon_{ci+pm}^* - \epsilon_{ow}^*}{\epsilon_{ci+pm}^* + 2\epsilon_{ow}^*} \right] \right) / \left(\left[\frac{r_{ow}}{r_{ci+pm}} \right]^3 - \left[\frac{\epsilon_{ci+pm}^* - \epsilon_{ow}^*}{\epsilon_{ci+pm}^* + 2\epsilon_{ow}^*} \right] \right) \tag{5}$$

where ci, pm and ow are the abbreviations of cell interior, plasma membrane and outer wall, respectively. The obtained ϵ_{cell}^* was substituted in Eq. 2 to calculate the f_{CM} of yeast cells. The $Re[f_{CM}]$ spectra of yeast cells, obtained by the above procedure, are shown in Fig. 4. The graph shows the $Re[f_{CM}]$ of the live and dead cells at medium conductivities of 0.001 and 0.14 S/m. The low medium conductivity was obtained using a solution of DI water (for the live cells) or DI water/methanol (for not stained dead cells), while the high medium conductivity was obtained by adding Trypan blue to the solution. According to this graph, at $\sigma_{medium} = 0.001$ S/m, the live cells behave positively over the whole frequency range whereas the dead

cells behave negatively at frequencies higher than 5.7 MHz. Alternatively, at $\sigma_{medium} = 0.14$ S/m, the live cells behave positively at frequencies higher than 2 MHz while the dead cells behave negatively over the whole frequency range. According to Fig. 4, the application of an AC signal at 20 MHz facilitates the separation of the live and dead cells at the both medium conductivities of 0.001 and 0.14 S/m.

4.2 Prediction of DEP forces on live and dead yeast cells

Applying the $Re[f_{CM}]$ from Fig. 4, the DEP force imposed on the live and dead cells was simulated throughout the microchannel. Figure 5 shows the distribution of DEP force at $z = 10 \mu\text{m}$ when $\sigma_{medium} = 0.14$ S/m, $V = 25$ V_{p-p} and $f = 20$ MHz. Figure 5a shows the DEP force vectors applied on live yeast cells. The live cells exhibited a positive DEP response at this medium conductivity with a $Re[f_{CM}] = 0.065$ (Fig. 4). The force vectors were directed towards the microelectrode and reached a maximum value of 2.2×10^{-11} N at the tips. The DEP- x force was much weaker than the drag force and could not affect the moving of cells along the x -axis, as observed in the experiments. In contrast, the DEP- y and DEP- z forces, which had similar magnitudes, could effectively induce lateral motions along the y and z axes. The DEP- y force pushed the live cells towards the inner edges of the microelectrodes while the DEP- z force pushed them downward. Under these two motions, the live cells would be accumulated between the microelectrode pairs, as will be shown in the experiments. Alternatively, Fig. 5b shows the DEP force vectors applied on dead yeast cells. The dead cells exhibited a negative DEP response at this medium conductivity with a $Re[f_{CM}] = -0.34$ (Fig. 4). The force vectors were directed away from

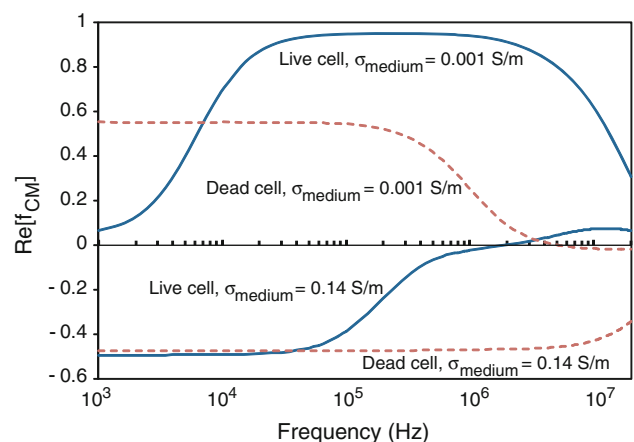


Fig. 4 The $Re[f_{CM}]$ spectra of live and dead yeast cells, obtained by double-shell model as given in Huang et al. (1992)

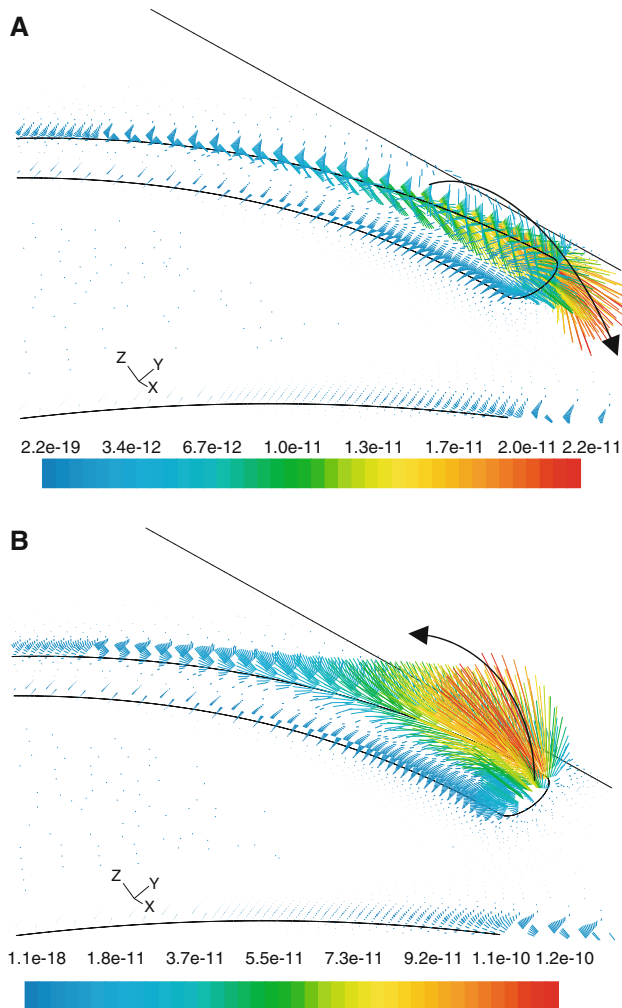


Fig. 5 The DEP forces (N) imposed on live and dead yeast cells at $\sigma_{\text{medium}} = 0.14$ S/m, $V = 25$ V_{p-p}, $f = 20$ MHz at $z = 10$ μm : **a** live cells exhibited positive DEP behaviour and were attracted towards the microelectrodes, and **b** dead cells exhibited negative DEP behaviour and were repelled from the microelectrodes

the microelectrode and reached a maximum value of 1.2×10^{-10} N at the tips, which was much stronger than that of the live cells. The DEP- y force pushed the dead cells away from the microelectrodes while the DEP- z force pushed them upward defying the sedimentation force. Under these two motions, the dead cells would be pushed towards the sidewalls and levitated within the microchannel.

5 Results

5.1 DEP manipulation of live yeast cells

Figure 6 shows the response of the live yeast cells at the consequent microelectrode pairs of the system. The flow

rate and conductivity of the medium were 1 $\mu\text{l}/\text{min}$ and 0.001 S/m, respectively, while the magnitude and frequency of the applied signal were 30 V_{p-p} and 20 MHz, respectively. At this frequency, the live cells demonstrated positive DEP behaviour, and were attracted towards the microelectrodes as predicted in Fig. 4. Reaching the microelectrodes, the live cells formed pearl chains under the growing electric field (Fig. 6a). The free ends of the cell chains were pushed towards the microelectrodes and were trapped along the surface. The cell chains were patterned along the electric field lines while their free ends attracted more cells to form a dense layer of trapped cells between the microelectrodes (Fig. 6a). The density of trapped cells increased along the microelectrodes due to their curved shape. Under the applied conditions, most cells were trapped before reaching the tips; however, on increasing the flow rate, the accumulated cells were shifted towards the tips. The cells, which remained in the flow, gradually lost their heights under the positive DEP- z force until being trapped by the next pair (Fig. 6b). The density of the trapped cells decreased considerably at the last microelectrode pair (Fig. 6c), since most cells had been trapped by the upstream pairs. Under the current settings, the cells that were moving far from the centreline ($y > 400$ μm) were not affected by the microelectrodes and kept moving under the drag force.

The DEP response of the live yeast cells was further analysed at the applied frequencies of 1,000, 50 and 15 kHz (Fig. 7). The images were taken from the first microelectrode pair 90 s after applying the AC signal. At 1 MHz, the cells accumulated persistently along the microelectrodes and formed a large mass of cells, which was extended ~ 915 μm off the microelectrode tip (Fig. 7a). Decreasing the frequency to 50 kHz, the cells accumulated at a lower rate and the extension of accumulated mass was decreased to ~ 370 μm (Fig. 7b). Finally, at 15 kHz, the cells lost their positive response and were not accumulated between the microelectrodes (Fig. 7c).

The DEP response of the live cells was also analysed at high medium conductivities of 0.14 and 0.25 S/m (not shown). The live cells demonstrated a crossover frequency of ~ 3 MHz at $\sigma_{\text{medium}} = 0.14$ S/m, below which they exhibited a negative DEP behaviour that is fairly consistent with Fig. 4. The difference between the calculated and observed crossover frequencies might be attributed to the asymmetric shape of cells, amplifying dipoles at both ends of the cell, which results in a higher crossover frequency. Conversely, at $\sigma_{\text{medium}} = 0.25$ S/m, the live cells demonstrated a negative DEP behaviour at all the frequencies.

It should be noted that exposing cells to electric fields could damage them. The cells trapped at the microelectrode edges under the positive DEP force are particularly at

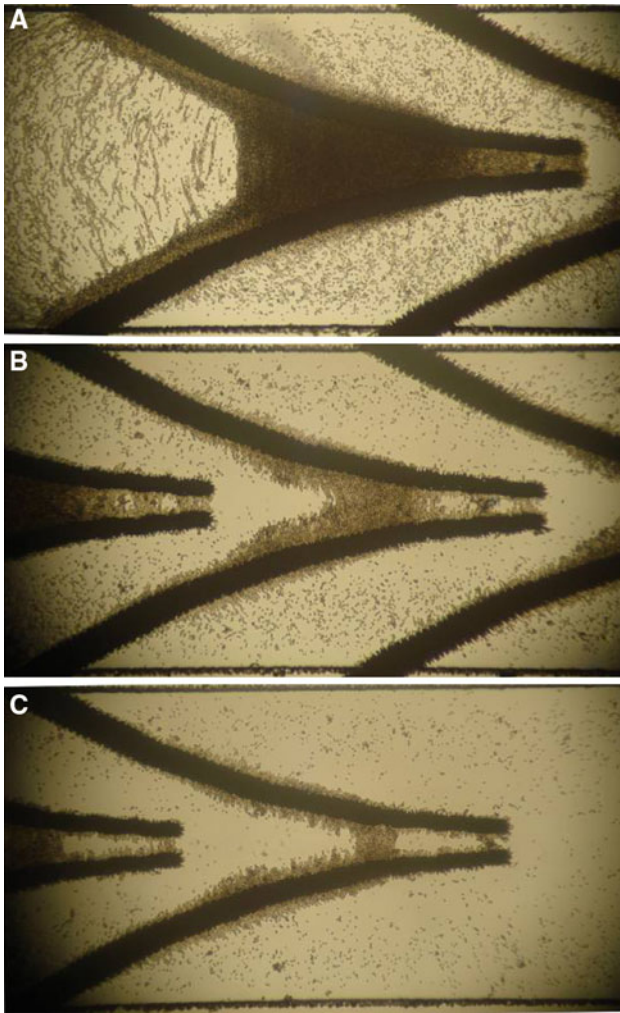


Fig. 6 The live yeast cells were trapped by consequent microelectrodes at $\sigma_{\text{medium}} = 0.001$ S/m: **a** first pair, **b** middle pair and **c** last pair of the sorting array

more risk since they are settled at the regions of highest electric field during the experiment (3–5 min). These cells might be damaged due to the electroporation of the cell membrane (Wang et al. 1999), imposing stress-related biological functions (Gambari et al. 2003), and activating membrane-bound proteins (Voldman 2006). Operating at low frequencies (not in the case of our study) initiates further toxic reactions between the cell and chemical species produced at the surface of the microelectrodes (Wang et al. 1999). However, the available data are not conclusive, and there are examples indicating the viability of red blood cells (Stephens et al. 1996) and yeast cells (Markx et al. 1994) after the DEP manipulation.

5.2 DEP manipulation of the dead yeast cells

Figure 8 shows the response of the dead yeast cells at the consequent microelectrode pairs of the system. The flow

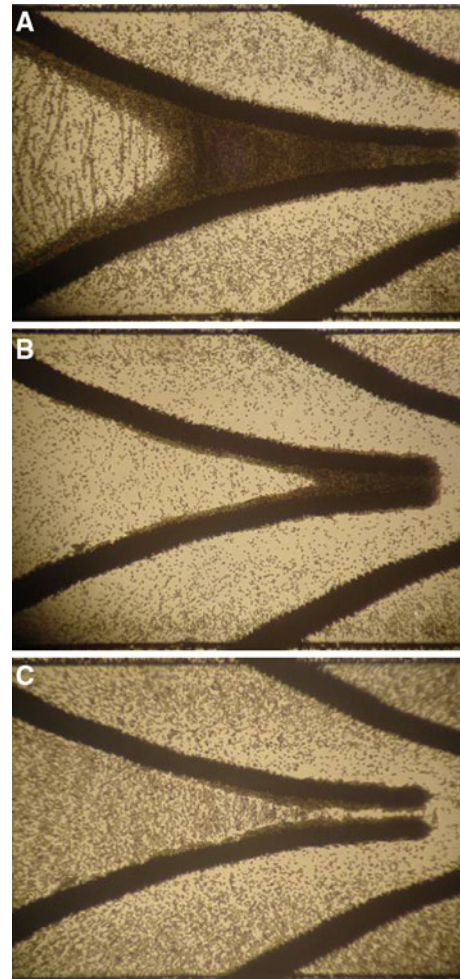


Fig. 7 At $\sigma_{\text{medium}} = 0.001$ S/m, while the live cells demonstrated positive DEP response throughout the frequency range, their trapment strongly depended on the applied frequency: **a** 1 MHz, **b** 50 kHz and **c** 15 kHz

rate and conductivities of the medium were $1 \mu\text{l}/\text{min}$ and 0.14 S/m, respectively, while the magnitude and frequency of the applied signal were $30 V_{\text{p-p}}$ and 20 MHz, respectively. The high medium conductivity was obtained after adding Trypan blue to the mixture of DI water/methanol to stain the dead cells. At this frequency, the dead cells demonstrated a negative DEP behaviour and were repelled from the microelectrodes as predicted in Fig. 4. According to Fig. 8, the cells that were moving far from the centreline ($y > 400 \mu\text{m}$) were not affected by the microelectrodes. Alternatively, the cells that were moving more closely to the centreline ($170 < y < 400 \mu\text{m}$) were pushed towards the sidewalls under the negative DEP- y force. These cells formed two thick strips at $y = \sim \pm 225 \mu\text{m}$, beyond which the cells marched along the microchannel (Fig. 8a). Instead, the cells that moved very closely to the centreline ($y < 170 \mu\text{m}$) were decelerated under the negative DEP force and funnelled between the microelectrodes.

Approaching the tips, most of these cells were deflected towards the sidewalls while a few of them were levitated to higher heights and formed two thick strips along the centreline (Fig. 8a). The strong levitation of these cells was observed by adjusting the microscope objective at different elevations of the microchannel. For example, in Fig. 8b, the objective was focused at higher elevations, and, hence, the microelectrodes and the cells moving close to the sidewalls became out of focus. The location of the cells was stabilized by the next microelectrode pairs (Fig. 8c).

The response of the dead yeast cells was further analysed at a low medium conductivity of 0.001 S/m and at different frequencies of 20, 7.5 and 5 MHz (Fig. 9). The images were taken at the last microelectrode pair to analyse

the overall performance of the system. At 20 MHz, the cells were repelled from the microelectrodes (Fig. 8a). In contrast to Fig. 8a, all the cells were pushed towards the sidewalls and were not funnelled along the centreline. Decreasing the frequency to 7.5 MHz, the negative response of cells weakened, and the cells could pass the microelectrode tips with less interruption. Finally, at 5 MHz, the cells exhibited a positive response and were trapped at the microelectrode edges (Fig. 9c). Further experiments revealed that the dead cells have a crossover frequency of ~ 6.5 MHz at this medium conductivity, fairly consistent with Fig. 4. Again, the difference between the calculated and the observed crossover frequencies might be due to the asymmetric shape of the cells, as mentioned before.

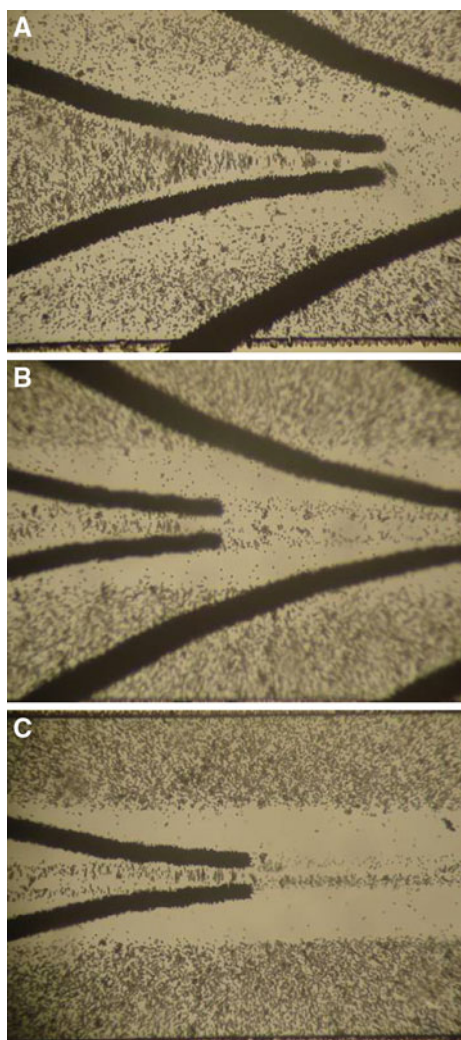


Fig. 8 The dead yeast cells were repelled from the consequent microelectrodes at $\sigma_{\text{medium}} = 0.14$ S/m: **a** first pair, **b** middle pair and **c** last pair of sorting array

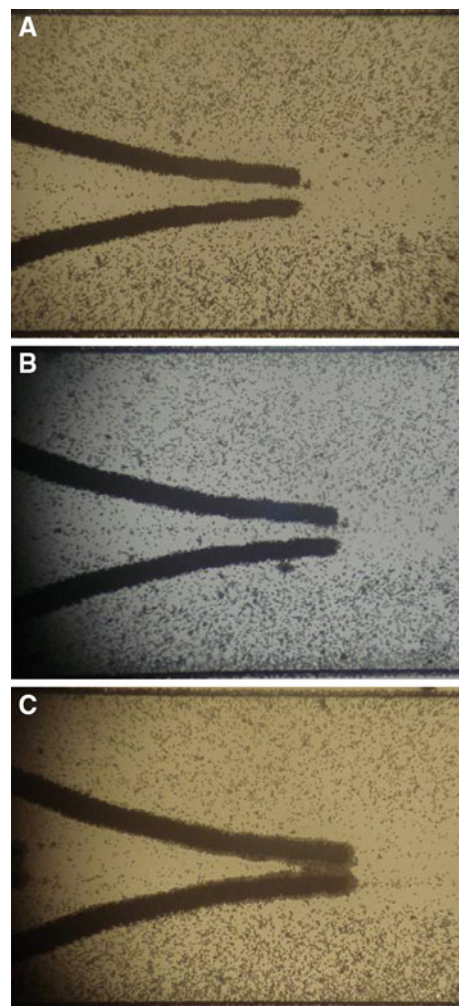


Fig. 9 The repelling of the dead cells strongly depended on the applied frequency. The dead cells had a crossover frequency of ~ 6.5 MHz at $\sigma_{\text{medium}} = 0.001$ S/m, for frequencies lower than that, the cells behaved positively, and were trapped by the microelectrodes: **a** 20 MHz, **b** 7.5 MHz and **c** 5 MHz

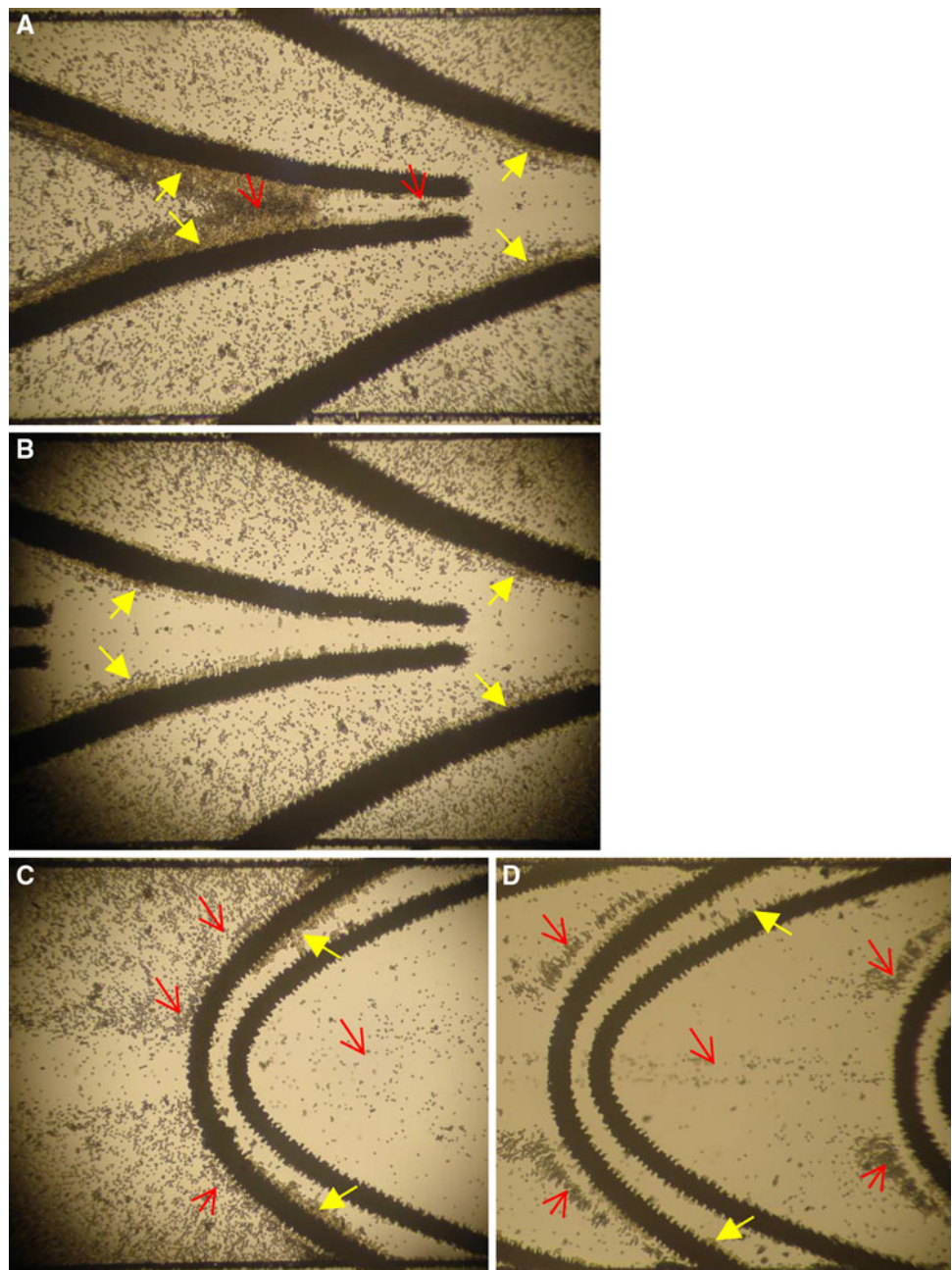
5.3 Separation of live and dead yeast cells

Figure 10 shows the separation of the live and dead yeast cells at a low medium conductivity of 0.001 S/m. The flow rate was decreased to 0.75 $\mu\text{l}/\text{min}$ to enhance the separation efficiency of the system while the magnitude and frequency of the applied signal were 30 V_{p-p} and 20 MHz, respectively. Figure 10 shows the first and last pairs of the sorting array as well as the first and second pairs of the assessing array. The first array sorted the live and dead cells whereas the second array assessed the sorting performance of the

system. For more clarification, the live and dead cells are marked with filled and hollow arrows, respectively.

In the sorting array, the live cells were trapped by the positive DEP forces and seen as a bright mass accumulated along the first pair of microelectrodes (Fig. 10a). Most of the live cells that were moving close to the centreline ($y < 400 \mu\text{m}$) were trapped by the upstream pairs and, hence, the density of trapped cells decreased significantly at the last pair of microelectrodes (Fig. 10b). Alternatively, the dead cells were repelled by the negative DEP forces. These cells were decelerated along the microelectrodes and

Fig. 10 The sorting of the live and dead cells by the DEP system at $\sigma_{\text{medium}} = 0.001 \text{ S/m}$. The first array sorted the live and dead cells whereas the second array assessed the sorting performance of the system: **a** first pair of the sorting array, **b** last pair of the sorting array, **c** first pair of the assessing array, where the remaining live cells were trapped between the pair while the dead cells were retained behind them and **d** the dead cells, which had passed through the first pair before activating the assessing array, were retained behind the consequent pairs (**d**). The live and dead cells are marked with filled and hollow arrows, respectively



seen as dark strips aligned parallel to the surface. Approaching the tips, the cells were pushed towards the sidewalls to create an almost cell-free region along the centreline (Fig. 10a).

After 5 min, when the system reached a stable condition, the assessing array was activated at $30 V_{p-p}$ and 20 MHz. The boomerang-shaped microelectrodes were excited with AC signal in an interdigitated manner. In doing so, the live cells that remained in the flow were accumulated between the boomeranged pairs under the positive DEP force. Experiments showed that the live cells were only trapped close to the sidewalls, indicating that all the live cells moving close to the centreline had been trapped by the sorting array (Fig. 10c). The density of the trapped cells over the second array increased very slowly with respect to time, which corresponded to the effective trapping performance of the sorting array. For example, Fig. 10c was taken 3 min after the activation of the assessing array. Alternatively, the dead cells were repelled from the boomerang-shaped microelectrodes under the negative DEP force and exhibited two different responses according to their locations across the microchannel. The dead cells that were moving close to the sidewalls were initially retained behind the first pair and seen as dark strips aligned parallel to the microelectrode (Fig. 10c). The boomerang-shaped pairs generated less repulsive force along the sidewalls where the gap between them reached a maximum value of $250 \mu\text{m}$. Therefore, the retained cells were further pushed towards the sidewalls under the drag force, where they were levitated and passed through the microelectrodes. This response avoided the blocking of the microchannel by the retained cells. Conversely, a few dead cells, which were moving closer to the centreline and levitated at higher heights, were not affected by the second array and passed through the barrier with no interruption (Fig. 10c). A portion of dead cells, which had passed through the first pair before activating the assessing array, were retained behind the consequent boomerang-shaped pairs (Fig. 10d).

The separation efficiency of the system was further evaluated by conducting Trypan blue exclusion assay. In this process, first, the assessing array was inactivated and the outlet flow of the system, which was supposed to contain dead cells, was collected in a syringe (BD plastic, 10). Second, the AC signal was inactivated and the live cells trapped by the microelectrodes were released and collected in another syringe. Third, the samples were introduced to the wells of a standard cell counting chamber (Neubauer hemocytometer) using a pipet. The cover slip of the chamber was divided into nine grids of 0.04 mm^2 . The number of non-stained (viable) and stained (non-viable) cells was counted in five different grids of the cover slip, under the microscope to calculate the percentage of the

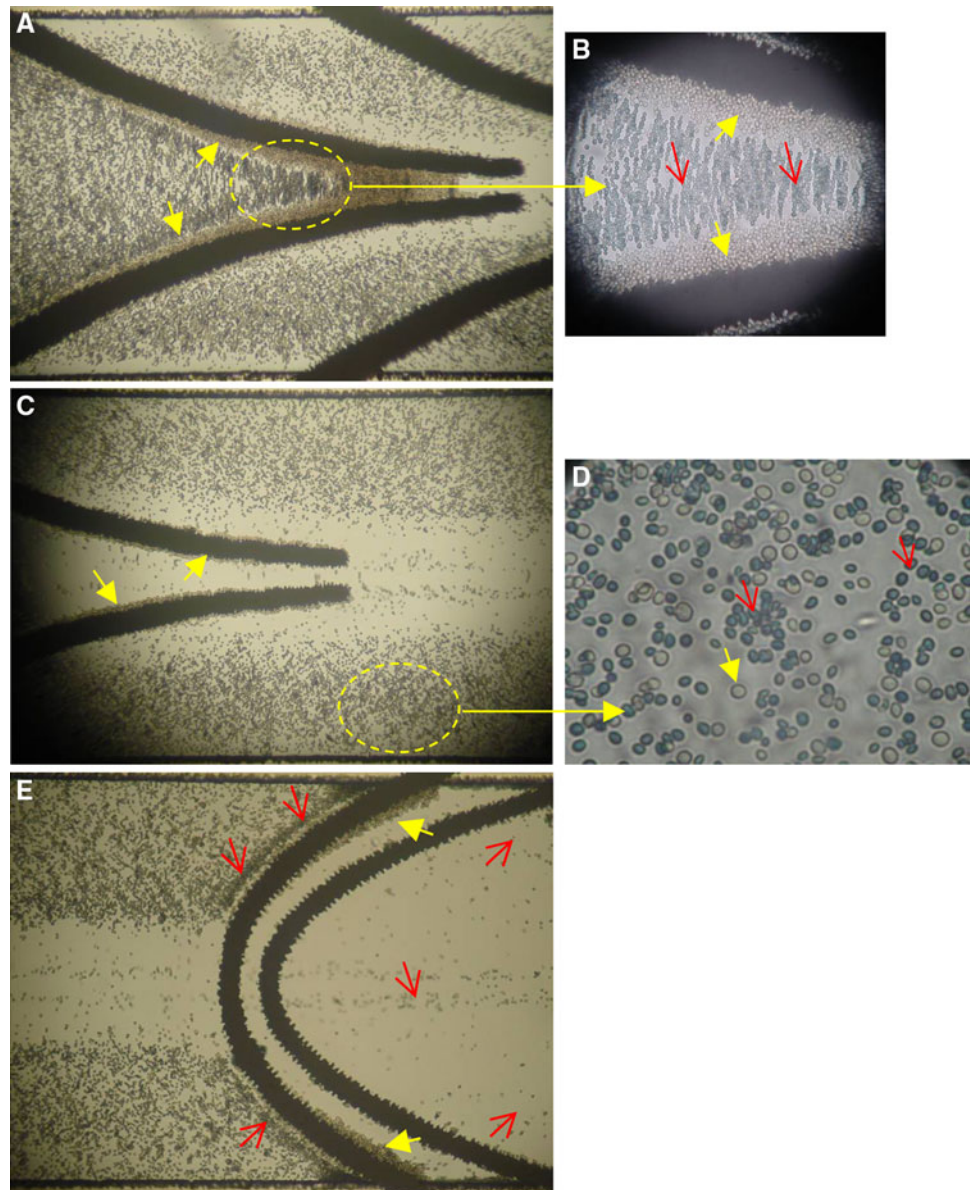
stained cells. This experiment was conducted on the live and dead samples separately, indicating that $\sim 85\%$ of the live sample cells were not stained (viable) while $\sim 75\%$ of the dead sample cells were stained (non-viable). Combining those two figures, the overall separation efficiency of the system was estimated as $\sim 80\%$ at this medium conductivity.

Further experiments at this medium conductivity revealed that the separation efficiency of the system strongly depends on the concentration of cells. Decreasing the total concentration of cells to 3.5×10^7 cell/ml (30% decreases) improved the separation efficiency of the live and dead cells to $\sim 88\%$ and $\sim 79\%$, respectively. In contrast, increasing the total concentration of cells to 6×10^7 cell/ml (20% increases) reduced the separating efficiency of the live and dead cells to $\sim 77\%$ and $\sim 70\%$, respectively. It is possible that high concentration of cells disrupts the distribution of electric field due to interference with a large number of cells, weakening the DEP forces. Moreover, it was observed that increasing the concentration of cells increases their affinity to the sidewalls, where the DEP forces are not strong enough to sort the cells.

The separation efficiency of the system could be improved by lowering the medium flow rate, since the cells were exposed to DEP forces for a longer time and could be manipulated more effectively. However, this strategy was not adopted due to the following reasons: (i) it decreased the throughput of the system; (ii) it exposed the cells to strong electric fields for a longer time and could deteriorate them; and (iii) it led to the domination of electro-convective forces at the tips, under which two vortices formed at the tips that interrupted the trapping of the live cells and created further chaotic motions within the microchannel.

Figure 11 shows the separation of the live and dead yeast cells at a high medium conductivity of 0.14 S/m . The live cells responded positively, and the dead cells responded negatively to the DEP field as predicted in Fig. 4. However, the positive response of the live cells was weakened due to the high conductivity of the medium, which, in turn, decreased the effective trapping portion of the microelectrodes. In order to compensate for this weakness, the flow rate of the solution was decreased to $0.6 \mu\text{l/min}$, and further, the magnitude of the applied signal was decreased to $25 V_{p-p}$ to diminish the electro-convective motions at the tips. Conversely, the negative response of the dead cells was boosted due to the high conductivity of the medium. The dead cells that were moving more closely to the centreline ($160 < y < 400 \mu\text{m}$) were pushed towards the sidewalls and formed two thick strips at $y = \sim \pm 180 \mu\text{m}$, beyond which the cells marched along the microchannel. Alternatively, the cells that were moving very closely to the centreline ($y < 160 \mu\text{m}$) were decelerated and funnelled between the microelectrodes.

Fig. 11 The sorting of live and dead cells by the DEP system at $\sigma_{\text{medium}} = 0.14 \text{ S/m}$: **a** the first pair of the sorting array, **b** the zoomed image shows the bright live cells that were trapped along the first microelectrode pair and the dark dead cells that were funnelled between them, **c** the last pair of the sorting array, **d** the zoomed image shows the cells that moving very close to sidewalls, revealing the low population of live cells even at this far region, and **e** the first pair of the assessing array, where the remained live cells were trapped between the pair while the dead cells were stopped behind them. Alternatively, the dead cells moving along the centreline passed the barrier. The live and dead cells are marked with filled and hollow arrows, respectively



Approaching the tips, most of these cells were pushed towards the sidewalls while a few of them were levitated to higher heights and moved along the centreline as two thick strips (Fig. 11a). The consequent microelectrodes stabilized the location of the dead cells within the microchannel (Fig. 11b).

After 5 min, when the system reached a stable condition, the assessing array was activated at $25 \text{ V}_{\text{p-p}}$ and 20 MHz. The live cells that remained in the flow were trapped by the assessing array (Fig. 11c). The live cells were only trapped close to the sidewalls, confirming that the live cells flowing close to the centreline were trapped. The dead cells that were moving along the centreline passed through the assessing array without interruption. Alternatively, the dead cells that were moving close to the sidewalls under the repulsive effect of the sorting array

were initially retained behind the first pair and then were dragged towards the sidewalls to pass through the assessing array (Fig. 11c).

Further microscopic cell counting indicated that $\sim 90\%$ of the live sample cells were not stained (viable) while $\sim 80\%$ of the dead sample cells were stained (non-viable). Combining those two populations, the overall separation efficiency of the system was estimated as $\sim 85\%$ at this medium conductivity.

The performance of DACS devices relies on several parameters of the system such as the magnitude of the applied AC signal, flow rate of the suspension, dielectric characteristics of the target cells, dimensions of the system and the number of microelectrode pairs involved. Therefore, all those parameters should be considered when comparing the sorting efficiency of DACS devices. In

doing so, the separation efficiency of our DACS device can be compared with those of (Gascoyne et al. 2009; Li and Bashir 2002; Moon et al. 2009; Pommer et al. 2008).

Compared with DACS device of Li and Bashir (2002), in which the live and heat-treated *Listeria* cells were separated with an efficiency of >90% by means of interdigitated microelectrodes in a stationary mode (zero flow), our system operates at 0.6 $\mu\text{l}/\text{min}$, and, therefore, can analyse larger volumes of target cells. Compared with DACS device of Pommer et al. (2008), in which platelets were sorted from diluted whole blood with an efficiency of $\sim 95\%$ by means of two arrays of oblique microelectrodes operating at 100 $V_{\text{p-p}}$, our system operates at 25–30 $V_{\text{p-p}}$, and, therefore, the likelihood of damaging of cells considerably decreases. Compared with DACS device of Gascoyne et al. (2009), in which circulating tumour cells were isolated from clinical blood specimens with an efficiency of >90% by utilizing vertical DEP-field flow fraction strategy (sorting the cells at different levitation heights to move at different velocities), our system relies on lateral DEP-field flow fraction strategy (sorting the cells at different locations across the microchannel width), which facilitates the real-time observation of cells by a conventional inverted microscope. Finally, compared with DACS device of Moon et al. (2009), in which airborne bacteria and polystyrene beads were separated with an efficiency of >90% by means of curved microelectrodes at a flow rate of 0.1 $\mu\text{l}/\text{min}$ (plus 0.4 $\mu\text{l}/\text{min}$ sheath flow), our system has a higher throughput of 0.6 $\mu\text{l}/\text{min}$.

Higher separation efficiencies can be achieved by reducing the inefficient sections of the microchannel that are close to the sidewalls and do not experience strong DEP forces. This goal can be achieved in several ways such as decreasing the width of the microchannel, introducing sheath flow to focus the cells along the centreline (Doh and Cho 2005; Moon et al. 2009) or implementing circular barriers within the microchannel along the sidewalls upstream of the microelectrodes to reroute the cells off the sidewalls (Khoshmanesh et al. 2008). The alternative strategy is to activate the assessing microelectrode array to act in conjunction with the sorting array. In this case, the live cells that have passed through the sorting array would be trapped along the sidewalls while the dead cells would pass through both arrays despite their local deceleration at the assessing array, as shown in Figs. 10 and 11.

5.4 Analysing the Joule heating effect

The generation of strong electric fields between the microelectrodes rises the flow temperature due to Joule heating effect (Cetin and Li 2008; Morgan and Green 2003). This temperature rise can be calculated using the energy balance equation of the flow, as described below.

The first term of this equation presents the heat dissipation due to thermal conduction, and the second term presents the heat generation due to Joule heating while the convective term is ignored due to the low velocity of the flow (Grom et al. 2006; Iliescu et al. 2009).

$$\nabla(k \cdot \nabla T) + \sigma E^2 = 0 \quad (6)$$

in which, k and σ are the thermal and electric conductivities of the flow, respectively.

The local temperature rise induces additional electrohydrodynamic (EHD) forces on the cells, which can be significant in highly conductive electrolytes. The average EHD force per unit volume of cells can be calculated as below (Morgan and Green 2003):

$$\begin{aligned} \bar{F}_{\text{EHD}} = & -0.5 \left(\frac{\partial \sigma}{\sigma \partial T} - \frac{\partial \varepsilon}{\varepsilon \partial T} \right) \nabla T \frac{\varepsilon \cdot E_{\text{rms}}^2}{1 + (\omega \tau)^2} \\ & + 0.25 \frac{\partial \varepsilon}{\partial T} \nabla T E_{\text{rms}}^2 \end{aligned} \quad (7)$$

where $\tau = \varepsilon/\sigma$ is the charge relaxation time of the liquid.

The values of electric field were substituted in Eq. 6 to obtain the temperature distribution of the flow. Our results indicated that a maximum temperature rise of 0.15 and 16.8°C occurred nearby the tips at the medium conductivities of 0.001 and 0.14 S/m, respectively. Figure 12a illustrates the temperature distribution of the medium at $z = 10 \mu\text{m}$ when $\sigma_{\text{medium}} = 0.14 \text{ S/m}$, $V = 25 V_{\text{p-p}}$ and $f = 20 \text{ MHz}$. Considering the system inlet temperature as 25°C, the local temperature reached 41.8°C at the tips. This high temperature does not damage the yeast cells, as they are quite resilient against temperature rise; however, it could lead to the death of mammalian cells since it is 4.8°C above their physiological temperature (37°C). According to our calculations, at medium conductivities <0.1 S/m the maximum temperature would be <38°C, which is a safe margin for the survival of mammalian cells (Voldman 2006).

Next, Eq. 7 was solved to calculate the average EHD force applied on the cells. In doing so, the medium's normalized temperature dependence of conductivity and permittivity of water were assumed as $(1/\sigma)(\partial \sigma/\partial T) = +0.02^\circ\text{C}^{-1}$ and $(1/\varepsilon)(\partial \varepsilon/\partial T) = -0.004^\circ\text{C}^{-1}$, respectively (Morgan and Green 2003). Figure 12b shows the average EHD force applied on yeast cells at $z = 10 \mu\text{m}$. The EHD force acted to repel the cells from the regions of high electric field and temperature, formed at the tips. In this sense, the EHD force opposed the positive DEP force, which acted to trap the live cells between the tips. Compared with Fig. 5a, the positive DEP force was 7.5 times stronger than the EHD force and still managed to accumulate the live cells nearby the tips, as confirmed by our experiments. Our experiments showed that increasing the magnitude of AC signal to 30 $V_{\text{p-p}}$ led to destabilizing the accumulation of the live cells and was prohibited at $\sigma_{\text{medium}} = 0.14 \text{ S/m}$.

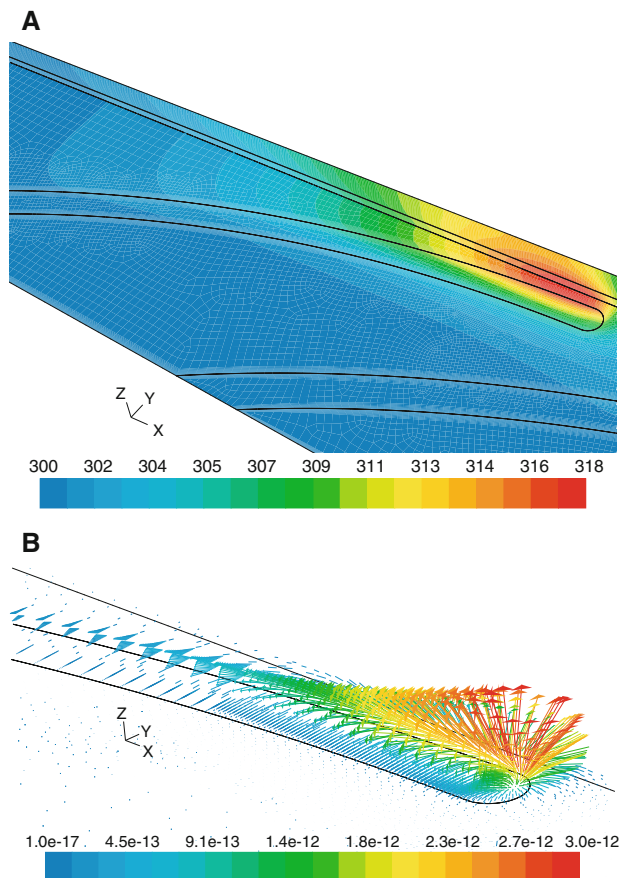


Fig. 12 The consequences of Joule heating phenomenon at $\sigma_{\text{medium}} = 0.14 \text{ S/m}$, $V = 25 \text{ V}_{\text{p-p}}$, $f = 20 \text{ MHz}$ at $z = 10 \mu\text{m}$: **a** the temperature of medium jumps to 43°C (316°K) between the microelectrodes, **b** the induced EHD forces reaches a maximum value of $3 \times 10^{-12} \text{ N}$ at the tips, which acts repels the cells from the microelectrode tips

6 Conclusion

In this study, we demonstrate the manipulation and separation of the live and dead yeast cells using dielectrophoresis. The DEP system utilizes two arrays of curved microelectrodes, in which the first array sorts the cells according to their DEP response while the second array examines the sorting efficiency. The live and dead cells exhibit both positive and negative responses at different medium conductivities and applied frequencies. The double-shell model of cell reveals that applying an AC signal at 20 MHz enables the separation of the live and dead cells at both medium conductivities of 0.001 and 0.14 S/m. The numerical simulations predict the responses of the live and dead cells prior to experiments. The performance of the system is initially assessed by manipulating the separate live and dead cell samples at different medium conductivities and applied frequencies. The system is later applied to separate the live and dead cells at the both mentioned medium conductivities. The microscopic cell counting experiment reveals a

separation efficiency of $\sim 80\%$ and $\sim 85\%$ at medium conductivities of 0.001 and 0.14 S/m, respectively. The separating efficiency of the device can be further improved by decreasing the width of the microchannel or increasing the magnitude of the applied AC signal. The proposed system is an effective platform to separate biological cells for purification, monitoring and diagnostic purposes.

References

- Abidin ZZ, Marx GH (2005) High-gradient electric field system for the dielectrophoretic separation of cells. *Journal of Electrostatics* 63(6–10):823–830
- Andersson H, van den Berg A (2003) Microfluidic devices for cellomics: a review. *Sens Actuat B* 92(3):315–325
- Arnold WM (2001) Positioning and levitation media for the separation of biological cells. *IEEE Trans Ind Appl* 37(5):1468–1475
- Arnold WM, Franich NR (2006) Cell isolation and growth in electric-field defined micro-wells. *Curr Appl Phys* 6(3):371–374
- Baratchi S, Kanwar RK, Khoshmanesh K, Vasu P, Ashok C, Hittu M, Parratt A, Krishnakumar S, Sun X, Kanwar JR (2009) Drug nanoshuttles to cross the blood brain barrier: promises of nanotechnology for drug delivery to the brain. *Curr Nanosci* 5(1):15–25
- Bhatt KH, Grego S, Velev OD (2005) An AC electrokinetic technique for collection and concentration of particles and cells on patterned electrodes. *Langmuir* 21(14):6603–6612
- Castillo J, Dimaki M, Svendsen WE (2009) Manipulation of biological samples using micro and nano techniques. *Integr Biol* 1(1):30–42
- Cetin B, Li DQ (2008) Effect of Joule heating on electrokinetic transport. *Electrophoresis* 29(5):994–1005
- Cetin B, Kang Y, Wu Z, Li D (2009) Continuous particle separation by size via AC-dielectrophoresis using a lab-on-a-chip device with 3-D electrodes. *Electrophoresis* 30(5):1–7
- Crane JS, Pohl HA (1968) A study of living and dead yeast cells using dielectrophoresis. *J Electrochem Soc* 115(6):584–586
- Dalton C, Goater AD, Burt JPH, Smith HV (2004) Analysis of parasites by electrorotation. *J Appl Microbiol* 96(1):24–32
- Doh I, Cho YH (2005) A continuous cell separation chip using hydrodynamic dielectrophoresis (DEP) process. *Sens Actuat A* 121(1):59–65
- El-Ali J, Sorger PK, Jensen KF (2006) Cells on chips. *Nature* 442(7101):403–411
- Fatoyinbo HO, Kamchis D, Whittingham R, Ogin SL, Hughes MP (2005) A high-throughput 3-D composite dielectrophoretic separator. *IEEE Trans Biomed Eng* 52(7):1347–1349
- Fu LM, Lee GB, Lin YH, Yang RJ (2004) Manipulation of microparticles using new modes of traveling-wave-dielectrophoretic forces: numerical simulation and experiments. *IEEE-ASME Trans Mechatron* 9(2):377–383
- Gambari R, Borgatti M, Altomare L, Manaresi N, Medoro G, Romani A, Tartagni M, Guerrieri R (2003) Applications to cancer research of “lab-on-a-chip” devices based on dielectrophoresis (DEP). *Technol Cancer Res Treat* 2(1):31–40
- Gascoyne PRC, Vykoukal JV (2004) Dielectrophoresis-based sample handling in general-purpose programmable diagnostic instruments. *Proc IEEE* 92(1):22–42
- Gascoyne P, Satayavivad J, Ruchirawat M (2004) Microfluidic approaches to malaria detection. *Acta Trop* 89(3):357–369
- Gascoyne PRC, Noshari J, Anderson TJ, Becker FF (2009) Isolation of rare cells from cell mixtures by dielectrophoresis. *Electrophoresis* 30(8):1388–1398

- Gray DS, Tan JL, Voldman J, Chen CS (2004) Dielectrophoretic registration of living cells to a microelectrode array. *Biosens Bioelectron* 19(7):771–780
- Grom F, Kentsch J, Muller T, Schnelle T, Stelzle M (2006) Accumulation and trapping of hepatitis A virus particles by electrohydrodynamic flow and dielectrophoresis. *Electrophoresis* 27(7):1386–1393
- Hashimoto M, Kaji H, Nishizawa M (2009) Selective capture of a specific cell type from mixed leucocytes in an electrode-integrated microfluidic device. *Biosens Bioelectron* 24(9):2892–2897
- Hoeb M, Radler JO, Klein S, Stutzmann M, Brandt MS (2007) Light-induced dielectrophoretic manipulation of DNA. *Biophys J* 93(3):1032–1038
- Hoettges KF, Dale JW, Hughes MP (2007) Rapid determination of antibiotic resistance in *E. coli* using dielectrophoresis. *Phys Med Biol* 52(19):6001–6009
- Holzel R (1997) Electrorotation of single yeast cells at frequencies between 100 Hz and 1.6 GHz. *Biophys J* 73(2):1103–1109
- Hu XY, Bessette PH, Qian JR, Meinhart CD, Daugherty PS, Soh HT (2005) Marker-specific sorting of rare cells using dielectrophoresis. *Proc Natl Acad Sci USA* 102(44):15757–15761
- Huang Y, Holzel R, Pethig R, Wang XB (1992) Differences in the AC electrodynamic of viable and nonviable yeast-cells determined through combined dielectrophoresis and electrorotation studies. *Phys Med Biol* 37(7):1499–1517
- Hunt TP, Lee H, Westervelt RM (2004) Addressable micropost array for the dielectrophoretic manipulation of particles in fluid. *Appl Phys Lett* 85(26):6421–6423
- Hunt TP, Issadore D, Westervelt RM (2008) Integrated circuit/microfluidic chip to programmably trap and move cells and droplets with dielectrophoresis. *Lab Chip* 8(1):81–87
- Iliescu C, Tresset G, Xu G (2009) Dielectrophoretic field-flow method for separating particle populations in a chip with asymmetric electrodes. *Biomicrofluidics* 3:044104
- Jones TB (2003) *Electromechanics of particles*. Cambridge University Press, Cambridge
- Kadaksham J, Singh P, Aubry N (2005) Dielectrophoresis induced clustering regimes of viable yeast cells. *Electrophoresis* 26(19):3738–3744
- Kalantar-zadeh K, Fry B (2007) *Nanotechnology enabled sensors*. Springer, New York
- Kang YB, Cetin B, Wu Z, Li D (2009) Continuous particle separation with localized AC-dielectrophoresis using embedded electrodes and an insulating hurdle. *Electrochim Acta* 54(6):1715–1720
- Khoshmanesh K, Kouzani AZ, Nahavandi S, Baratchi S, Kanwar JR (2008) At a glance: cellular biology for engineers. *Comput Biol Chem* 32(5):315–331
- Khoshmanesh K, Zhang C, Tovar-Lopez FJ, Nahavandi S, Baratchi S, Kalantar-zadeh K, Mitchell A (2009) Dielectrophoretic manipulation and separation of microparticles using curved microelectrodes. *Electrophoresis* 30(21):3707–3717
- Kononenko VL, Shimkus JK (2000) Stationary deformations of erythrocytes by high-frequency electric field. *Bioelectrochemistry* 52(2):187–196
- Krassowska W, Neu JC (1994) Response of a single cell to an external electric field. *Biophys J* 66(6):1768–1776
- Kua CH, Lam YC, Rodriguez I, Yang C, Youcef-Toumi K (2007) Dynamic cell fractionation and transportation using moving dielectrophoresis. *Anal Chem* 79(18):6975–6987
- Kuzyk A, Yurke B, Toppari JJ, Linko V, Torma P (2008) Dielectrophoretic trapping of DNA origami. *Small* 4(4):447–450
- Lee K, Kwon SG, Kim SH, Kwak YK (2007) Dielectrophoretic tweezers using sharp probe electrode. *Sens Actuat A* 136(1):154–160
- Li H, Bashir R (2002) Dielectrophoretic separation and manipulation of live and heat-treated cells of *Listeria* on microfabricated devices with interdigitated electrodes. *Sens Actuat B* 86(2–3):215–221
- Li YL, Dalton C, Crabtree HJ, Nilsson G, Kaler K (2007) Continuous dielectrophoretic cell separation microfluidic device. *Lab Chip* 7(2):239–248
- Markx GH, Talary MS, Pethig R (1994) Separation of viable and nonviable yeast using dielectrophoresis. *J Biotechnol* 32(1):29–37
- Moon HS, Nam YW, Park JC, Jung HI (2009) Dielectrophoretic separation of airborne microbes and dust particles using a microfluidic channel for real-time bioaerosol monitoring. *Environ Sci Technol* 43(15):5857–5863
- Morales FHF, Duarte JE, Martí JS (2008) Non-uniform electric field-induced yeast cell electrokinetic behaviour. *Revista Ingenieria E Investigacion* 28(3):116–121
- Morgan H, Green N (2003) *AC electrokinetics: colloids and nanoparticles*. Research Studies Press, Baldock
- Morgan H, Hughes MP, Green NG (1999) Separation of submicron bioparticles by dielectrophoresis. *Biophys J* 77(1):516–525
- Morgan H, Sun T, Holmes D, Gawad S, Green NG (2007) Single cell dielectric spectroscopy. *J Phys D* 40(1):61–70
- Neek-Amal M, Lajevardipour A, Sepangi HR (2009) Electric field effects on nano-scale bio-membrane of spherical cells. *Physica A* 388(2–3):120–128
- Pethig R, Talary MS (2007) Dielectrophoretic detection of membrane morphology changes in Jurkat T-cells undergoing etoposide-induced apoptosis. *IET Nanobiotechnol* 1(1):2–9
- Pommer MS, Zhang YT, Keerthi N, Chen D, Thomson JA, Meinhart CD, Soh HT (2008) Dielectrophoretic separation of platelets from diluted whole blood in microfluidic channels. *Electrophoresis* 29(6):1213–1218
- Radu M, Ionescu M, Irimescu N, Iliescu K, Pologea-Moraru R, Kovacs E (2005) Orientation behavior of retinal photoreceptors in alternating electric fields. *Biophys J* 89(5):3548–3554
- Roda B, Zatonni A, Reschiglian P, MM H, Mirasoli M, Michelini E, Roda A (2009) Field-flow fractionation in bioanalysis: a review of recent trends. *Anal Chim Acta* 635(2):132–143
- Sanchis A, Brown AP, Sancho M, Martinez G, Sebastian JL, Munoz S, Miranda JM (2007) Dielectric characterization of bacterial cells using dielectrophoresis. *Bioelectromagnetics* 28(5):393–401
- Stephens M, Talary MS, Pethig R, Burnett AK, Mills KI (1996) The dielectrophoresis enrichment of CD34(+) cells from peripheral blood stem cell harvests. *Bone Marrow Transplant* 18(4):777–782
- Uppalapati M, Huang YM, Jackson TN, Hancock WO (2008) Microtubule alignment and manipulation using AC electrokinetics. *Small* 4(9):1371–1381
- Urdaneta M, Smela E (2007) Multiple frequency dielectrophoresis. *Electrophoresis* 28(18):3145–3155
- Voldman J (2006) Electrical forces for microscale cell manipulation. *Annu Rev Biomed Eng* 8:425–454
- Wang XJ, Yang J, Gascoyne PRC (1999) Role of peroxide in AC electrical field exposure effects on Friend murine erythroleukemia cells during dielectrophoretic manipulations. *Biochim Biophys Acta* 1426(1):53–68
- Wang ZY, Hansen O, Petersen PK, Rogeberg A, Kutter JP, Bang DD, Wolff A (2006) Dielectrophoresis microsystem with integrated flow cytometers for on-line monitoring of sorting efficiency. *Electrophoresis* 27(24):5081–5092
- Zhang C, Khoshmanesh K, Tovar-Lopez FJ, Mitchell A, Kalantar-zadeh K (2009) Dielectrophoretic separation of carbon nanotubes and polystyrene microparticles. *Microfluid Nanofluid* 7(5):633–645
- Zhang C, Khoshmanesh K, Mitchell A, Kalantar-zadeh K (2010) Dielectrophoresis for the manipulation of micro/nano particles in microfluidic systems. *Anal Bioanal Chem* 396(1):401–420